

## Variation of the Lateral Mobility of Transmembrane Peptides with Hydrophobic Mismatch

Yann Gambin,<sup>†</sup> Myriam Reffay,<sup>†</sup> Emma Sierecki,<sup>‡</sup> Fabrice Homblé,<sup>§</sup> Robert S. Hodges,<sup>||</sup> Nir S. Gov,<sup>⊥</sup> Nicolas Taulier,<sup>▽, #</sup> and Wladimir Urbach<sup>\*, †</sup>

Laboratoire de Physique Statistique, Ecole Normale Supérieure, UPMC Univ Paris 6, Université Paris Diderot, CNRS, 24 rue Lhomond, 75005 Paris, France, Synthèse et Structure de Molécules d'Intérêt Pharmacologique, UMR8638 (CNRS-Université Paris Descartes), 4 av. de l'Observatoire, 75006 Paris, France, Structure and Function of Biological Membranes, Université Libre de Bruxelles, CP206/2 Campus Plaine, 1050 Bruxelles, Belgique, and Department of Biochemistry and Molecular Genetics, University of Colorado at Denver, Colorado 80004, Department of Chemical Physics, The Weizmann Institute of Science, Rehovot, Israel 76100, Laboratoire d'Imagerie Paramétrique, UMPC Paris, UMR 7623, Paris, France, and CNRS, UMR 7623, Paris, France

Received: November 30, 2009; Revised Manuscript Received: January 14, 2010

A hydrophobic mismatch between protein length and membrane thickness can lead to a modification of protein conformation, function, and oligomerization. To study the role of hydrophobic mismatch, we have measured the change in mobility of transmembrane peptides possessing a hydrophobic helix of various length  $d_\pi$  in lipid membranes of giant vesicles. We also used a model system where the hydrophobic thickness of the bilayers,  $h$ , can be tuned at will. We precisely measured the diffusion coefficient of the embedded peptides and gained access to the apparent size of diffusing objects. For bilayers thinner than  $d_\pi$ , the diffusion coefficient decreases, and the derived characteristic sizes are larger than the peptide radii. Previous studies suggest that peptides accommodate by tilting. This scenario was confirmed by ATR-FTIR spectroscopy. As the membrane thickness increases, the value of the diffusion coefficient increases to reach a maximum at  $h \approx d_\pi$ . We show that this variation in diffusion coefficient is consistent with a decrease in peptide tilt. To do so, we have derived a relation between the diffusion coefficient and the tilt angle, and we used this relation to derive the peptide tilt from our diffusion measurements. As the membrane thickness increases, the peptides raise (i.e., their tilt is reduced) and reach an upright position and a maximal mobility for  $h \approx d_\pi$ . Using accessibility measurements, we show that when the membrane becomes too thick, the peptide polar heads sink into the interfacial region. Surprisingly, this “pinching” behavior does not hinder the lateral diffusion of the transmembrane peptides. Ultimately, a break in the peptide transmembrane anchorage is observed and is revealed by a “jump” in the  $D$  values.

## Introduction

It has been shown that variation of membrane thickness modulates the activity of pore-forming proteins such as gramicidin<sup>1</sup> and proteins with tilted transmembrane segments such as rhodopsin.<sup>2</sup> Molecular<sup>3–5</sup> and continuum<sup>6,7</sup> models predicted that the lipid or membrane properties play a significant role in transmembrane protein function. In addition, the energetic cost of local mismatch between protein height and the lipid bilayer can also drive membrane reorganization, sorting proteins in adapted microdomains. Thus theoretical and experimental interest has turned toward the effects of mismatch between the hydrophobic length of transmembrane  $\alpha$ -helices of integral proteins and the hydrophobic thickness of membranes.<sup>8</sup> Various peptides have been designed along the years to mimic the hydrophobic segments of membrane proteins.<sup>9</sup> They are usually made of a single transmembrane  $\alpha$ -helix. The orientation of these peptides in mismatched conditions has been explored

through a variety of techniques: NMR, X-ray, circular dichroism, Fourier transform infrared spectroscopy, electron spin resonance, and molecular simulations.<sup>10–19</sup> All these studies agree that when the membrane thickness is smaller than the transmembrane segment, the peptide accommodates by tilting. However, the extent of tilt remains controversial, and the experimental measurement of the peptide angle is not straightforward since most techniques required perfectible models as recently shown for NMR.<sup>20–22</sup> The peptide behavior is more uncertain when the hydrophobic bilayer thickness is larger than the hydrophobic peptide length. Several studies suggest that the peptide “snorkels” to some extent, and others hypothesize that the lipid mattress adjusts itself through large deformation around the peptide.<sup>8,16,23,24</sup> For a very strong mismatch, peptides may not be able to span the membrane anymore<sup>25</sup> and could lie at the hydrophobic–hydrophilic interface.<sup>17,18</sup> In this case, it could be difficult to experimentally separate insertion defects due to protocols of peptide incorporation and mechanistic/energetic impossibility for the peptide to insert correctly within the bilayer. The use of model bilayer composed of surfactants, swollen by hydrophobic solvents, can be advantageously used to successfully insert the peptides before increasing the mismatch.<sup>25,26</sup>

It was previously believed that the size of a transmembrane object could not be deduced from mobility measurements, as the theoretical work of Saffman and Dellbrück<sup>27</sup> predicted that,

\* Author to whom correspondence may be addressed. E-mail: urbach@lps.ens.fr.

<sup>†</sup> Ecole Normale Supérieure.

<sup>‡</sup> Université Paris Descartes.

<sup>§</sup> Université Libre de Bruxelles.

<sup>||</sup> University of Colorado at Denver.

<sup>⊥</sup> The Weizmann Institute of Science.

<sup>▽</sup> UMPC Paris.

<sup>#</sup> CNRS, UMR 7623, LIP.

within a layer of incompressible fluid, the diffusion coefficient should be insensitive to the size of the diffusing object. Consequently, studies of lateral mobility have neglected model systems<sup>28</sup> where little information should be obtained, and focused on living cells<sup>29–31</sup> to explore the mechanical barriers hindering the movement of proteins. The validity of the Saffman–Dellbrück (SD) model has never been adequately verified because of a lack of systematic measurements. Lee and Petersen<sup>32</sup> first clearly pointed out the inability of the SD model to describe their measurements of the diffusion coefficient of various peptide aggregates. More recently, we demonstrated that diffusion coefficients  $D$  of transmembrane proteins within lipid or surfactant bilayers are in fact inversely proportional to their radius  $R$ , following a “Stokes–Einstein” law:<sup>33,34</sup>

$$D = \frac{k_B T}{4\pi} \times \frac{\lambda}{\mu_m} \times \frac{1}{hR} \quad (1)$$

where  $h$  is the hydrophobic thickness of the bilayer,  $\mu_m$  the bilayer viscosity, and  $\lambda$  a characteristic length. This model perfectly described the size-dependence behavior of the diffusion coefficient of transmembrane peptides and small proteins, with radii  $R$  between 5 and 30 Å, observed by the authors and in previously published data. A more recent investigation by Kriegsman et al.<sup>35</sup> still confirms the  $1/R$  dependence of the diffusion coefficient using dual-focus FCS (fluorescence correlation spectroscopy). Surprisingly, Ramadurai et al.,<sup>36</sup> using a simpler one-focus FCS, could not observe this behavior. A theoretical work from Naji et al.<sup>34</sup> recently explained the reason for the failure of the Saffman–Delbrück model, which predicted a weak  $D(R)$  variation. The SD model does not take into account an enhanced dissipation arising from lipids around the transmembrane protein, the properties of which are different from those of lipids far away from the protein. Naji et al. hypothesized that only membrane deformation due to mismatch modifies lipid properties. However, experiments based on tryptophan fluorescence measurements showed that about 15 lipids are disturbed by transmembrane peptides in matching conditions.<sup>19</sup> We may hypothesize that, in eq 1,  $\lambda$  is the length over which the enhanced dissipation occurs or alternately the distance over which lipid properties are modified due to the presence of the transmembrane protein or peptide.

In the present article we have precisely measured the diffusion coefficient  $D$  of peptides of various hydrophobic lengths inserted either in lipid or surfactant bilayers. The latter bilayer can be swollen with oil in order to modulate its hydrophobic thickness. Using this system, we have investigated the behavior of the diffusion coefficient under hydrophobic mismatch.

## Materials and Methods

The model peptides  $L_n$  are constituted of a polyleucine stretch of increasing hydrophobic length ( $n = 12, 18,$  or  $24$  residues), capped on one or both ends by polar heads, as sketched and described in Figure 1. The sequences of polyleucine create robust and well-characterized hydrophobic  $\alpha$ -helices of radius  $R_p = 5.5$  Å; the anchoring to the surface of the bilayer is ensured by positively charged lysine residues. Their hydrophobic length  $d_\pi$  is derived using a helix translation of 1.5 Å per leucine residue. These peptides were synthesized and purified as trifluoroacetic acid (TFA) salts, using previously published solid-phase synthesis and reversed phase high-performance liquid chromatographic procedures.<sup>37–39</sup> They were labeled with a fluorescent group (FITC, fluorescein isothiocyanate) for diffu-

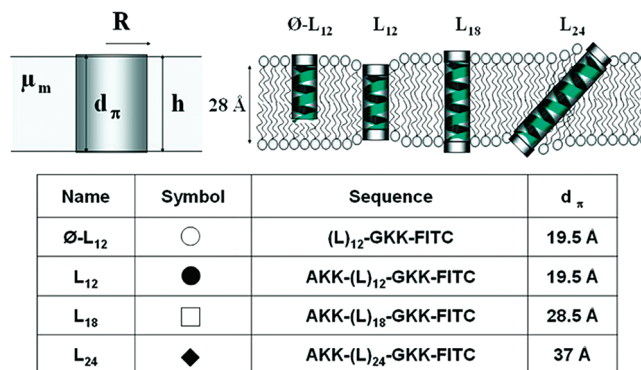


**Figure 1.** The table summarizes the properties of the peptides used in this work. The polyleucine cores are designed to form maximally stable  $\alpha$ -helices; their hydrophobic length  $d_\pi$  are calculated using a helix translation of 1.5 Å per residue. The top panel illustrates the parameters used in our model (eq 1) and the possible conformation of the peptides in the SOPC bilayer ( $h = 28$  Å).

sion measurements. The peptides were inserted in model bilayers made either from SOPC (stearyl-oleoyl-phosphatidylcholine) or from C<sub>12</sub>E<sub>5</sub> (penta-monododecyl ether). SOPC was purchased from Avanti Polar Lipids (Alabaster, AL) and C<sub>12</sub>E<sub>5</sub> from Nikkol (Japan). Both compounds were used without further purification. The SOPC bilayers form GUVs (giant unilamellar vesicles) and have a hydrophobic thickness of  $h = 28$  Å. The insertion of peptides in these GUVs follows previously published procedures.<sup>35</sup> The nonionic surfactant C<sub>12</sub>E<sub>5</sub> bilayers are self-organized in a sponge phase, the properties<sup>29</sup> of which were systematically checked by SAXS experiments. The sponge phases are prepared by simply mixing together the different components (that is C<sub>12</sub>E<sub>5</sub> surfactant,  $\beta$ -OG cosurfactant, water, and dodecane) at the desired concentrations. Dodecane is an aliphatic chain that matches the surfactant aliphatic chain length and is confined between the two surfactant monolayers. To avoid insertion defects, the peptides were incorporated into a solution of C<sub>12</sub>E<sub>5</sub>/ $\beta$ -OG/water; dodecane was then added in a step-by-step process.

SAXS measurements were performed using a rotating anode generator. The Cu–K $\alpha_1$  wavelength (1.54 Å) was selected by a gold-coated quartz mirror. The scattering intensity was recorded as a function of the scattering vector  $q (= 4\pi \sin(\theta)/\lambda)$  using a detector with a spatial resolution of 0.2 mm. The distance from the detector to the sample was 770 mm. The final resolution of the setup was 0.02 nm. Samples were placed in sealed glass capillaries and positioned in a thermostatted holder ( $T = 296$  K). All spectra exhibited a broad peak that indicated the characteristic distance  $d_B = 2\pi/q_{\max}$ . The oil-swollen bilayers thickness  $\delta$  is derived from water dilution measurements.<sup>40</sup> The hydrophobic membrane thickness,  $h$ , is eventually obtained by subtracting twice the length of the surfactant polar head,  $\delta_p = 16$  Å, to  $\delta$ . In each sample, the membrane thickness is perfectly controlled and can be progressively swollen by simply adding more dodecane during the sample preparation.

We use pattern photobleaching under a microscope to follow the self-diffusion of the labeled peptides in bilayers. The FRAPP technique is described in detail elsewhere;<sup>41–43</sup> it differs from the FRAP (fluorescence recovery after photobleaching) technique by the use of a fringe interference pattern rather than a confocal spot. Briefly, when illuminated by a high intensity laser flash (200 mW), the fluorescent labels are irreversibly bleached. The recovery of fluorescence intensity  $I(t)$  in the bleached areas is governed by the self-diffusion of the probes (Figure 2a). Recorded by a photomultiplier,  $I(t)$  follows in all our samples a monoexponential recovery in a characteristic recovery time

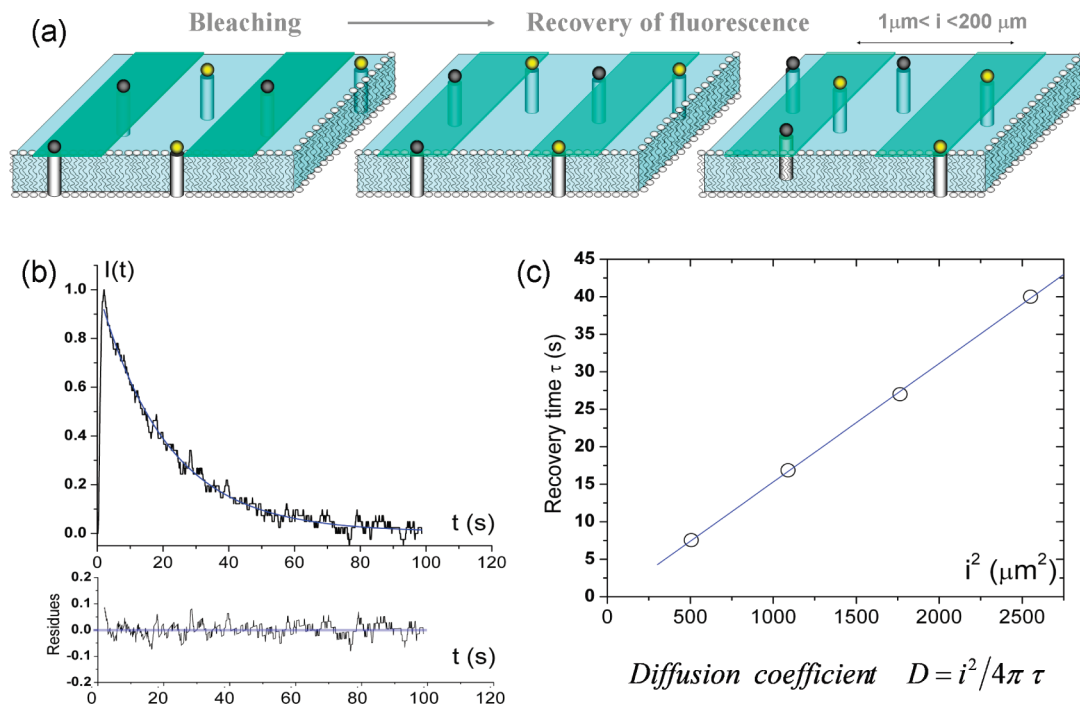


**Figure 2.** (a) The top panel illustrates the fluorescence recovery after pattern photobleaching (FRAPP) technique. The fluorescent labels grafted on the peptides are irreversibly bleached by a short laser flash. The intensity of fluorescence  $I(t)$  in the bleached areas recovers because of the self-diffusion of the peptides. (b)  $I(t)$  follows a monoexponential recovery with a characteristic time  $\tau$ , which depends on the size of the bleached area (fringe size  $i$ ) and of  $D$ . The systematic use of at least four fringe size allows us to check the Brownian diffusion of all peptides and to obtain the diffusion coefficient  $D$  with a precision better than 2%.

$\tau$ :  $I(t) = I_0 e^{-t/\tau}$  (Figure 2b), where  $I_0$  is a constant. In order to improve the signal-to-noise ratio, we use a fringe pattern, created by two laser beams intersecting exactly in the focal plane of an inverted light microscope (Leica DRMIB). The measurements performed in the sponge phase utilize the full volume of the 3  $\mu\text{L}$  sample that is introduced into 200  $\mu\text{m}$  deep glass microchannels by suction.

In order to measure the diffusion on the surface of lipid vesicles, we used an evanescent-wave modification of our setup. The two laser beams are coupled with the glass coverslip using a hemispherical prism (Edmund Optics microlens). Both beams reach the surface at the critical angle of reflection. This allows us to measure lateral diffusion in the upper most layers of the sample. Giant unilamellar vesicles were introduced into a chamber made with two coverslips sealed by a silicone gasket. First, a dilute solution of GUVs made of SOPC, with no fluorescent peptides, was used to wash the chamber. These vesicles will explode at the glass surface, effectively coating the chamber to prevent adhesion of the GUVs containing the fluorescent peptides that are introduced in a second step. The osmotic pressure and density of the buffer contained inside the GUVs has been adjusted to be 5–8% smaller than the medium filling the chamber. As a result, GUVs will ascend and come in contact with the SOPC-coated coverslip at the top of the chamber. The difference of osmotic pressure will make them slightly floppy and allow them to spread on the top surface, forming a large, flat surface of contact. Because there is no direct contact between the bilayer and the glass surface, the peptides are diffusing freely. The larger GUVs were selected for measurements, i.e., the GUVs presenting a flat area wider than 40  $\mu\text{m}$  in diameter. Thanks to the evanescent-wave illumination, the diffusion of the peptides is measured only in the flat section of the vesicles.

The systematic use of at least four interfringe sizes  $i$  ( $1 \mu\text{m} < i < 10 \mu\text{m}$  for GUVs,  $10 \mu\text{m} < i < 200 \mu\text{m}$  for sponge phase)

allows us to check that all peptides exhibit a Brownian diffusion and therefore obtain the diffusion coefficient  $D$  from  $D = i^2 / (4\pi^2\tau)$ , with a precision better than 2% (Figure 2c). Each set of FRAPP experiments was repeated five times, and the averaged results show extremely limited dispersion.

In the present work, we focus on effects arising from independent peptide diffusion: the use of lysine residues inhibits lateral association, and the peptides were incorporated at a minimal concentration. Typically for one peptide,  $10^4$ – $10^6$  lipids are used in the bilayers. Diffusion coefficient measurements performed on samples with increasing peptide concentration revealed no peptide aggregation in this concentration range. In all experiments we observed a pure monoexponential recovery of fluorescence, indicating monodisperse objects.

## Results

We used  $\alpha$ -helical peptides composed of a hydrophobic core of leucine repeats of variable length (12, 18, or 24 leucines) flanked by one (peptide  $\emptyset$ -L<sub>12</sub>) or two hydrophilic heads (peptides L<sub>12</sub>, L<sub>18</sub>, and L<sub>24</sub>). All peptides were labeled with FITC.

For each peptide, we prepare solutions of giant unilamellar vesicles (GUVs) where the fluorescent peptides were incorporated into the SOPC bilayer of GUVs. In each sample, we measure by FRAPP technique a single diffusion coefficient, the values of which are listed in Figure 3f. We observed that the peptide L<sub>18</sub>, that is best adapted to the bilayer ( $h = d_\pi$ ), possesses the highest mobility. The mobility of L<sub>24</sub> is decreased by 30% compared to the diffusion of L<sub>18</sub>. Surprisingly, while L<sub>12</sub> is supposed to pinch the bilayer, its diffusion coefficient is close to the one obtained for L<sub>18</sub>,  $D(\text{L}_{12}) \approx D(\text{L}_{18})$ . The fact that  $\emptyset$ -L<sub>12</sub>, which has only one polar head, diffuses faster than L<sub>12</sub> suggests that the latter is still anchored in both leaflets of the bilayer, while pinching it. We performed ATR-FTIR experiments in oriented lipid bilayers containing L<sub>18</sub> or L<sub>24</sub> to measure the

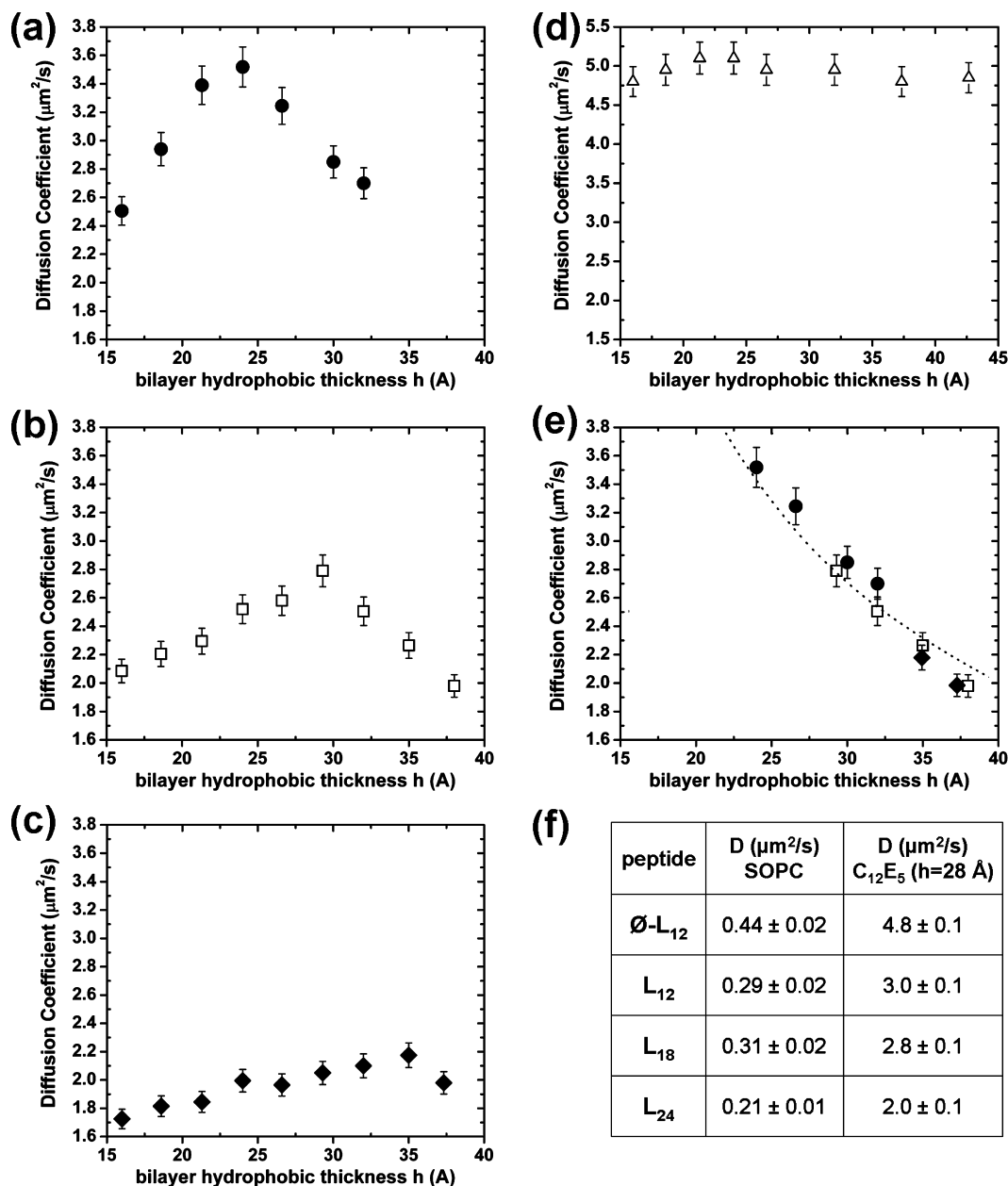


**Figure 3.** Diffusion coefficients  $D$  as a function of  $\text{C}_{12}\text{E}_5$  bilayer thickness  $h$  obtained for L<sub>12</sub> (a), L<sub>18</sub> (b), L<sub>24</sub> (c), and SOPC-NBD (d). For bilayers thicker than the peptide length  $d_p$ , a common behavior appears, correctly described by a  $1/h$  variation (dotted line, panel e). For each peptide, five sets of experiments allow us to obtain average values with reproducibility better than 5%. The table (f) gives the measured diffusion coefficient of these peptides in single giant unilamellar vesicle (GUV) made of SOPC. The diffusion coefficient was determined using evanescent FRAPP technique; data were averaged over 200 vesicles typically. The next column shows for comparison the diffusion estimated for the same peptides in  $\text{C}_{12}\text{E}_5$  bilayers of the same thickness as SOPC.

peptide tilt into SOPC bilayers. All absorbance results exhibit a narrow symmetric amide I signal centered at about  $1656\text{--}1658\text{ cm}^{-1}$ , characteristic of  $\alpha$ -helices (Figure 4). Furthermore, the data indicate that whereas the L<sub>18</sub> peptide is standing in an upright position ( $\theta = 0^\circ$ ), L<sub>24</sub> is tilted at  $18^\circ$  to the normal to the lipid bilayer.

Rather than synthesizing new peptides of intermediate length, to further check and interpret these results, we incorporated the same peptides in model, tunable bilayers made of a nonionic surfactant  $\text{C}_{12}\text{E}_5$ . In such a system, a hydrophobic mismatch is easily achieved by modulating the surfactant bilayer thickness, from  $h = 16$  up to  $40$  Å, by addition of a hydrophobic solvent. These model bilayers are self-organized in a multiconnected structure called “sponge” or L<sub>3</sub> phase. Since the FRAPP technique measures the long-range diffusion and the peptides

travel on distances as large as  $100\ \mu\text{m}$  in the phase, the peptide diffusion averages rapidly the local structures and random organization of the bilayers. The experiments conducted in these “melted cubic phases” lead to an excellent reproducibility between measurements, contrary to those performed in lamellar phases where orientation defects can appear.

In order to verify that the presence of dodecane does not affect the bilayer, we have measured the respective diffusion coefficients of a labeled surfactant ( $\text{C}_{12}$ -FITC) and a labeled lipid (SOPC-NBD). The labeled surfactant and lipid inserts in one monolayer (of hydrophobic thickness  $8$  Å). The length of the hydrophobic chain of the labeled surfactant matches the one of  $\text{C}_{12}\text{E}_5$ , whereas the lipid hydrophobic tails protrude by  $6$  Å. Consequently, the  $\text{C}_{12}$ -FITC molecule never interacts with the mid-plane dodecane upon swelling, whereas SOPC-NBD mol-

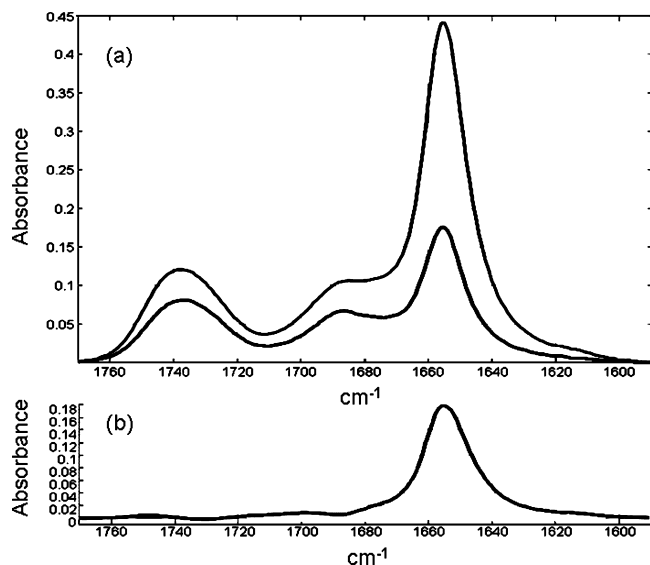


**Figure 4.** (a) ATR-FTIR spectra of  $L_{24}$  for parallel and perpendicular orientation of the polarizer (upper and lower curve, respectively). (b) The dichroic spectrum ( $\parallel - \perp$ ) was calculated using the carbonyl band of the lipid ( $1738 \text{ cm}^{-1}$ ) as a scaling factor. The positive peak of the  $\alpha$  helix shown in the dichroic spectrum indicates that the peptide is inserted in the lipid bilayer. The orientation of the peptide was calculated from the dichroic ratio ( $R^{\text{ATR}}_{1738} = 1.46$ ;  $R^{\text{ATR}}_{1655} = 2.77$ ) using a standard procedure.<sup>51,52</sup>

ecule does. The measured diffusion coefficients of both probes remain constant whatever the membrane thickness:  $D(\text{C}_{12}\text{-FITC}) = 8 \pm 0.2 \mu\text{m}^2/\text{s}$  and  $D(\text{SOPC-NBD}) = 5 \pm 0.2 \mu\text{m}^2/\text{s}$ . The swelling by dodecane has no apparent effect (Figure 3).

We measured the diffusion coefficient from the three transmembrane peptides  $L_{12}$ ,  $L_{18}$ , and  $L_{24}$ . All diffusion coefficients exhibit very similar behavior as shown in Figure 3: their diffusion is first accelerated and then hindered as the membrane is continuously swollen. As summarized in the table Figure 3f, the  $D$  values are significantly larger in  $\text{C}_{12}\text{E}_5$  than in SOPC bilayers. However, for the same bilayer thickness ( $h = 28 \text{ \AA}$ ) the same relative variations are measured. All three peptides reach a maximum diffusion for a membrane thickness close to their calculated hydrophobic length  $d_\pi$ . For  $L_{24}$ ,  $D$  reaches a maximum for  $h \approx 36 \text{ \AA}$ , that matches the peptide hydrophobic length  $d_\pi = 37 \text{ \AA}$ . For  $L_{18}$ , the maximum is obtained for  $h \approx 29 \text{ \AA}$ , while  $d_\pi = 28 \text{ \AA}$ . For the shorter peptide  $L_{12}$ , there is however a slight difference between its theoretical length  $d_\pi = 19.5 \text{ \AA}$  and the position of the maximum observed (about  $22 \text{ \AA}$ ). Among different suggestions advanced to explain this last discrepancy, the hypothesis of flexibility of the polar head seems the most reasonable. Killian and co-workers<sup>8,44</sup> have indeed shown that the lysine residues can exhibit a “snorkeling” behavior<sup>24</sup> that may displace the effective position of the polar head toward the aqueous medium.  $L_{12}$  may not be the “perfect ruler” in the thinnest bilayers. It must be emphasized that this 10% discrepancy represents only 1 to 2  $\text{\AA}$  on each side of the bilayer for  $L_{12}$ . For further considerations and calculations, we will therefore consider the “effective” length  $d_\pi$  of the peptide, as defined experimentally by the position of the maxima: 22, 29, and 36  $\text{\AA}$ , respectively, for  $L_{12}$ ,  $L_{18}$ , and  $L_{24}$ .

## Discussion

(i)  $h = d_\pi$ . **Determination of  $\lambda/\mu_m$ .** In our measurements made on lipid vesicles, the peptide  $L_{18}$  is in hydrophobic matching conditions: the FTIR spectra shows no tilt angle for

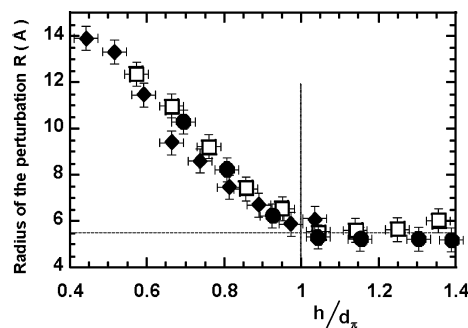


**Figure 5.** Effective radius  $R$  of the diffusing peptide versus relative mismatch  $h/d_\pi$  for the three peptides spanning the membrane,  $L_{12}$  (●),  $L_{18}$  (□), and  $L_{24}$  (◆). The peptide radius  $R_p$  is estimated to 5.5  $\text{\AA}$ .

this peptide that also possesses the highest diffusion coefficient value. In the measurements made on  $\text{C}_{12}\text{E}_5$  bilayers, all peptides reach a maximum mobility at hydrophobic matching condition, where peptides are expected to be cylinders of constant radius  $R_p = 5.5 \text{ \AA}$  that stands in an upright position into the bilayers. Considering our data at  $h = d_\pi$ , we observed in Figure 3e that for transmembrane peptides of same size  $R = R_p$ , the diffusion coefficient only depends on the hydrophobic bilayer thickness  $h$ .

In eq 1, the values of the length  $\lambda$  and of the membrane viscosity  $\mu_m$  are unknown. However, the ratio  $\lambda/\mu_m$  can be determined at  $h = d_\pi$ , as all other parameters are known. For a SOPC bilayer, the data for peptide  $L_{18}$  gives  $\lambda/\mu_m = (0.14 \pm 0.05) \times 10^{-8} \text{ mPa}^{-1} \text{ s}^{-1}$ , whereas for a  $\text{C}_{12}\text{E}_5$  bilayers all peptides lead to the same value  $\lambda/\mu_m = (1.35 \pm 0.05) \times 10^{-8} \text{ mPa}^{-1} \text{ s}^{-1}$ . This last result is a further piece of evidence that the properties of the  $\text{C}_{12}\text{E}_5$  bilayer are not affected by its swelling. If as a first approximation we suppose that the length  $\lambda$  is of the same order in lipid and in surfactant bilayers, then the difference in the value of  $\lambda/\mu_m$  suggests that a lipid bilayer is ten times more viscous than a surfactant bilayer. This result shows that the value of  $\lambda/\mu_m$  is characteristic of the bilayer properties, and that it is not possible to directly compare absolute values of diffusion coefficient measured from different bilayers.

Knowing the ratio  $\lambda/\mu_m$ , we can calculate an effective radius  $R$  of the peptide in hydrophobic mismatch conditions. Using an error propagation analysis, we estimate the error made on  $R$  values to be smaller than 0.5  $\text{\AA}$ . The calculated effective radius  $R$  is plotted versus the relative mismatch  $h/d_\pi$  in Figure 5 for  $L_{12}$ ,  $L_{18}$ , and  $L_{24}$  in  $\text{C}_{12}\text{E}_5$  bilayers. All the data collapse on a master curve. In the following, we explain the meaning of the changes in diffusion coefficient and its associated effective radius for positive and negative mismatch.

(ii)  $h > d_\pi$ : **Transmembrane to Membrane Transition.** We start from a swollen bilayer which hydrophobic thickness,  $h$ , matches the hydrophobic peptide length,  $d_\pi$ . When the membrane thickness increases, the mobility of the three transmembrane peptides is hindered in a common behavior:  $D \propto 1/h$  (see Figure 3). For the peptide  $L_{12}$ , we observe in Figure 6 a jump in its diffusion coefficient at  $h > 35 \text{ \AA}$ . In the same figure, we have displayed the diffusion coefficient of peptide  $\emptyset\text{-}L_{12}$ , which was constructed as a  $L_{12}$  deprived of one polar head. This peptide is structurally unable to anchor in both leaflets of the bilayer.  $\emptyset\text{-}L_{12}$  is not slowed down for  $h > d_\pi$  but rather reaches its maximum mobility when its hydrophobic segment is no longer in contact with the opposite monolayer, i.e., for  $h \approx d_\pi + 8 \text{ \AA} = 28 \text{ \AA}$ . The difference between  $D(\emptyset\text{-}L_{12})$  and  $D(L_{12})$  persists until  $h$  reaches the value  $h_c = d_\pi + 10 \text{ \AA}$ , where the diffusion coefficient of the transmembrane  $L_{12}$  peptide experiences a

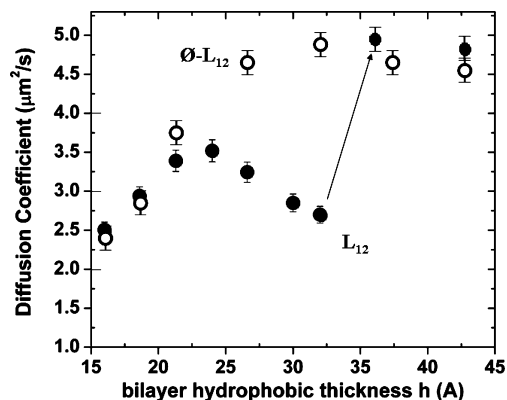


**Figure 6.** Comparison of the  $D(h)$  evolution of  $\text{\O-L}_{12}$  (○) and  $L_{12}$  (●) peptides. The “jump” experienced by  $L_{12}$  suggests that the anchorage on one side is lost (see text for details).

sudden jump. A similar transition was observed with  $L_{18}$  at  $h_c \approx d_\pi + 10 \text{ \AA} = 38 \text{ \AA}$  (not shown). The  $D$  variation of both peptides proves that the “jump” is a signature of a transmembrane anchoring. The peptide “pinching” behavior shows here its limits, contrary to what was observed for the leucine transmembrane peptide in the lamellar phase made of dodecane-swollen  $\text{C}_{12}\text{E}_4$  bilayers.<sup>22</sup> In addition, the jump in diffusion coefficient values is observed sooner ( $d_\pi + 7 \text{ \AA}$ ) in PBS buffer (pH 8) than in pure water ( $d_\pi + 10 \text{ \AA}$ ) for  $L_{12}$ . This is consistent with the fact that at higher pH, the lysine residues are deprotonated, lowering the energetic cost of translocation inside the membrane. The fact that  $D(L_{12}) = D(\text{\O-L}_{12})$  for  $h > h_c$  suggests that the effective radii of  $L_{12}$  and  $\text{\O-L}_{12}$  are identical. We hypothesize that  $L_{12}$  is standing in an upright position like that of  $\text{\O-L}_{12}$  peptide and does not lie on one monolayer surface as observed by Ren et al.<sup>17,18</sup> for short peptides inserted in lipid bilayers. Single-molecule pulling experiments are currently being performed on this system to quantify this phenomenon.

To further assess the pinching behavior of the transmembrane peptide during membrane swelling and the loss of the peptide transmembrane property at  $h > h_c$ , we have performed accessibility measurements using soluble fluorescent streptavidin proteins and biotinylated and nonfluorescent analogues of  $L_{12}$  and  $\text{\O-L}_{12}$  peptides (Figure 8). In these measurements, we follow the variations of the streptavidin diffusion coefficient. If streptavidin does not bind a biotinylated peptide, it will have the diffusion coefficient of a free streptavidin. If streptavidin binds a biotinylated peptide, its diffusion coefficient will be similar to the diffusion coefficient of the peptide. In the absence of peptide, our measurements show that streptavidin exhibits a single diffusion coefficient equal to  $D_S = D_{S,\text{free}} = 50 \mu\text{m}^2/\text{s}$  whatever the bilayer thickness,  $h$ . This high value reflects a three-dimensional diffusion where streptavidin interacts weakly with the bilayers. In the presence of  $\text{\O-L}_{12}$ , the diffusion coefficient of streptavidin is reduced to  $D_S = D(\text{\O-L}_{12})$  whatever  $h$ , indicating that streptavidin is constantly grafted to the peptide. In the presence of  $L_{12}$  and for  $h < d_{\text{eff}} = 22 \text{ \AA}$ ,  $D_S = D(L_{12})$ , indicating that streptavidin is bound to the tilted  $L_{12}$ . For bilayer thicknesses between 25 and 30  $\text{\AA}$ , the diffusion coefficient is equal to  $D_{S,\text{free}}$ , the streptavidin does not bind anymore the biotin attached to  $L_{12}$ . This result is consistent with a model where the peptide pinches the membrane, as sketched in Figure 8. In this model, the polar head of the peptide, where the biotin is attached, would “sink” inside the bilayer, out of reach of the streptavidin. As  $\text{\O-L}_{12}$  is not a transmembrane peptide, its conformation does not vary with the bilayer thickness and the biotin is accessible at all times.

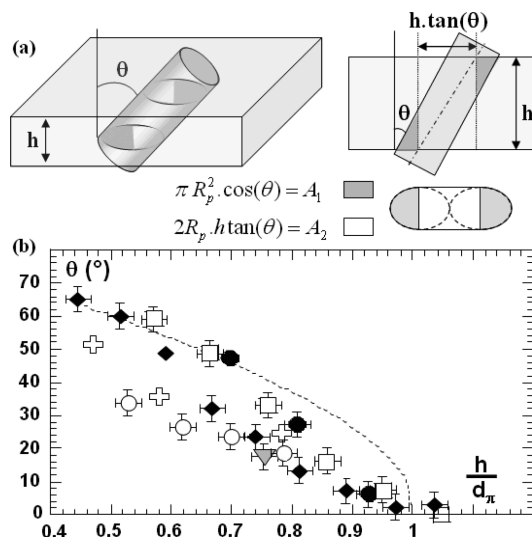


**Figure 7.** (a) Sketch of the geometrical model used to estimate the projected area of the tilted peptide:  $A_1$  oblate parts at the surface (gray) and  $A_2$  area of the projected section of the cylinder (empty). (b) Tilt angles  $\theta$  for  $L_{12}$  (●),  $L_{18}$  (□), and  $L_{24}$  (◆), versus the relative mismatch  $h/d_\pi$ .  $\theta$  is calculated from the radii of perturbation  $R_p$  of Figure 5 by solving the equation  $\pi R_p^2 = A_1 + A_2$  (see text). The gray symbol (▼) places the result obtained with  $L_{24}$  in SOPC. For comparison sake, cross symbol and values (○) are extracted from experiments and molecular simulations.<sup>48–50</sup> The dashed line represents the variations expected from the geometrical law  $\cos \theta = h/d_\pi$ .

Upon swelling, the hindrance to the diffusion arises from the changes in bilayer thickness, with no apparent increase in the effective radius (Figure 5). This result suggests that either the membrane deformation annulus is too small to be detected, or the perturbation exists but does not contribute efficiently to hinder the diffusion, because the surfactant molecules in the annulus are constantly regenerated and exchanged with those further away. This last suggestion agrees with the view of Naji et al.:<sup>34</sup> the surfactants or lipids do not change the apparent size  $R$  of the diffusing object, but rather contribute to the characteristic length  $\lambda$  through enhanced dissipation.

**(iii)  $h < d_\pi$ . Tilt of Peptides.** Investigations performed on peptides inserted into a membrane with a negative hydrophobic mismatch show that the peptide always accommodates by tilting.<sup>10–19</sup> The tilt angle  $\theta$  is defined as the angle between the bilayer normal and the peptide cylinder axis. The measurement of  $\theta$  is not an easy task. It has been performed by various authors either experimentally or numerically. The corresponding literature data are displayed in Figure 7 as a function of the relative mismatch  $h/d_\pi$ . The tilt angle linearly varies with the relative mismatch but does not follow the ideal geometric model  $\cos \theta = h/d_\pi$ , based on the hypothesis that there is no membrane or peptide deformation. We measured by FTIR a tilt angle  $\theta = 18^\circ$  for  $L_{24}$  in SOPC vesicles that is in good agreement with the linear behavior of literature data (Figure 6). We observe that the tilted ( $L_{24}$ ) and nontilted ( $L_{18}$ ) peptides in SOPC bilayers possess significantly different values of diffusion coefficient (Figure 3f): according to eq 1 the effective radius  $R$  of the tilted peptide is larger. Our result suggests that the effective radius is somehow related to tilt angle. If we consider transmembrane peptide to be roughly a cylinder of radius  $R_p = 5.5 \text{ \AA}$ , the effective size of the peptide can be represented by the surface area of a disk:  $S_{\text{eff}} = \pi R^2$ . Meanwhile, the peptide projected surface area (Figure 7a) is:

$$S = (2R_p \times h \times \tan(\theta)) + 2 \times (2\pi \times R_p \times \cos(\theta))$$

Since a tilted peptide is constantly moving around the bilayer normal, the projected surface  $S$  can be averaged as an effective surface of a disk:  $S = S_{\text{eff}}$ . Finally, the tilt angle can be extracted from our diffusion coefficient measurements using eq 1 and eq 2

$$2R_p \times [h \times \tan(\theta) + \pi R_p \times \cos(\theta)] = \pi R^2 \quad (2)$$

(see Appendix for an alternate but equivalent model). Using the value  $D(L_{24})$  in SOPC bilayer, one deduces from eq 1 that  $L_{24}$  occupies an effective radius of 8.1 Å (Figure 3f) which leads (using eq 2) to a tilt angle of 19° (Figure 7b) in good agreement with our FTIR estimation of 18°. Our results show that the value of diffusion coefficient is sensitive to peptide tilt and that the tilt angle can be derived from diffusion experiments.

In our experiments made on surfactant bilayers, we expect all peptides to be tilted in dry bilayers ( $h = 16$  Å). As dodecane is added, the peptide tilt should be reduced and eventually disappears at  $h = d_\pi$ . We observed a significant variation in diffusion coefficient induced by the hydrophobic mismatch. As the mismatch decreases, the lateral size of the peptide decreases as shown in Figure 5. Using eqs 1 and 2, we can relate these changes in lateral size to modifications in tilt angles for peptides  $L_{12}$ ,  $L_{18}$ , and  $L_{24}$  (Figure 7). For strong mismatch conditions ( $h/d_\pi < 0.7$ ), the results are well fitted by the simple geometrical evolution  $\cos \theta = h/d_\pi$  but not at small mismatched, where the data follow the linear behavior seen for lipid bilayers (Figure 7b). This last behavior suggests that the peptides recover more rapidly a vertical position. The difference observed between lipid and surfactant bilayers may come from the fact that surfactant bilayers are much more flexible than lipid bilayers. For a large mismatch, the high flexibility of the surfactant explains the validity of the observed geometrical evolution. For a small mismatch, dodecane can easily accumulate around the peptide to allow the bilayer to increase its thickness. Therefore, the tilt needed to relieve the slightly smaller mismatch would be reduced. However, the exact mechanism by which the peptide tilts and the bilayer accommodates the peptide could be resolved probably only through dynamic molecular simulation.

## Conclusion

We have precisely measured by FRAPP technique the variations of the diffusion coefficient of transmembrane helical peptide model bilayers, in hydrophobic mismatched conditions. We use lipid and surfactant bilayers. In the first system, the bilayer thickness is constant and the mismatch is achieved by changing the peptide length. In the second system, the bilayer thickness can be swollen by oil. Our measurements show that the value of the diffusion coefficient is very sensitive to hydrophobic mismatch. We could calculate the effective radius of the peptides using the newly proposed Stokes–Einstein-like equation. The mobility of transmembrane peptides is maximal at matching conditions, and a peptide moving in a single monolayer goes faster than a peptide bridging two monolayers. The peptide mobility decreases progressively when the mismatch increases. For a bilayer thickness larger than the peptide length, the peptide pinches the bilayer. Its effective radius does not change and the decrease in mobility is only due to the increase in bilayer thickness. If the bilayer becomes too thick, the peptide cannot span the bilayer anymore and diffuses on a single monolayer. When the peptide length is larger than the membrane

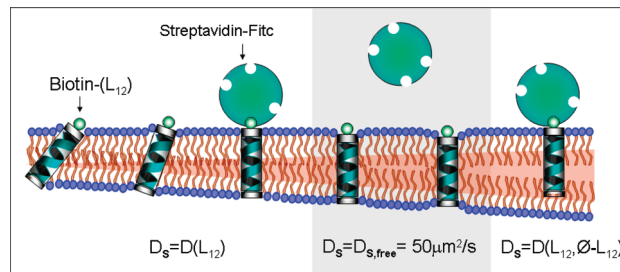


**Figure 8.** Using biotinylated  $L_{12}$  peptides and fluorescent streptavidin, we test the accessibility of the peptide polar head. The interaction between the streptavidin and the peptide considerably hinders the diffusion of the soluble streptavidin: its coefficient of diffusion drops from  $50 \mu\text{m}^2/\text{s}$  to a few  $\mu\text{m}^2/\text{s}$ . The  $D_s$  obtained matches the one obtained for  $L_{12}$ , except in a regime where the peptide seems to pinch the bilayer.

thickness, the variations in diffusion coefficient are consistent with a peptide tilt. Using a simple model, we could extract the peptide tilt angle from our diffusion measurements. We showed that the peptides can tilt up to 65°. As new methods allow the reconstitution of active proteins in model bilayers such as in GUVs,<sup>45–47</sup> the technique used here should accelerate the exploration of various phenomena such as lipid–protein interactions, amphipatic peptide assemblies, and pore formation.

**Acknowledgment.** This work was supported by a ACI-DRAB grant (no 04 2312) from the French Ministry of Research and a grant (eFFFLUX) from ANR.

## Appendix

### Alternate Model

We may rewrite eq 1 as

$$D = (kBT\lambda)/(2\mu_m S) \quad (3)$$

where  $S$  is the membrane surface area involved in the peptide friction. For a ratio  $\lambda/\mu_m$  that is not significantly altered under hydrophobic mismatch, we can calculate the hydrophobic friction area  $S$  from the measured diffusion coefficient. For an upright peptide in matching conditions,  $S$  perfectly matches the hydrophobic surface area of the peptide embedded in the hydrophobic part of the membrane, that is  $S_0 = 2\pi R_p d_\pi$ . In this case, eqs 3 and 1 are equivalent since  $R = R_p$  and  $h = d_\pi$ .

For  $h/d_\pi^{\text{eff}} > 1$ , for a tilted peptide that rapidly rotates, it sweeps a cylindrical volume inside the membrane whose surface is given by  $S = 2\pi h(R_p + h \tan \theta)$ . Using this last equation in combination with eq 3, we can extract the tilt angle from the measured diffusion coefficient.

For  $h/d_\pi^{\text{eff}} > 1$ , the derived surface area remains constant and appears to be equal to  $S = 2\pi R_p h$ . This means that although the real length of the peptide is smaller than the layer thickness, the shell where the momentum is dissipated is that of a cylinder with the full thickness of the membrane, presumably due to the pinching effect.

## References and Notes

- (1) Kelkar, D. A.; Chattopadhyay, A. *Biochim. Biophys. Acta* **2007**, *1768*, 1103–1113.
- (2) Botelho, A. V.; Huber, T.; Sakmar, T. P.; Brown, M. F. *Biophys. J.* **2006**, *91*, 4464–4477.
- (3) Duque, D.; Li, X. J.; Katsov, K.; Schick, M. *J. Chem. Phys.* **2002**, *116*, 10478–10484.
- (4) Fattal, D. R.; Benschaul, A. *Biophys. J.* **1993**, *65*, 1795–1809.

- (5) Fattal, D. R.; Benschaul, A. *Phys. A* **1995**, *220*, 192–216.
- (6) ArandaEspinoza, H.; Berman, A.; Dan, N.; Pincus, P.; Safran, S. *Biophys. J.* **1996**, *71*, 648–656.
- (7) Mouritsen, O.; Bloom, M. *Biophys. J.* **1984**, *46*, 141–153.
- (8) de Planque, M. R. R.; Killian, J. A. *Mol. Membr. Biol.* **2003**, *20*, 271–284.
- (9) Davis, J. H.; Clare, D. M.; Hodges, R. S.; Bloom, M. *Biochemistry* **1983**, *22*, 5298–5305.
- (10) Belohorcova, K.; Davis, J. H.; Woolf, T. B.; Roux, B. *Biophys. J.* **1997**, *73*, 3039–3055.
- (11) Belohorcova, K.; Qian, J.; Davis, J. H. *Biophys. J.* **2000**, *79*, 3201–3216.
- (12) Caputo, G. A.; London, E. *Biochemistry* **2003**, *42*, 3275–3285.
- (13) de Planque, M. R. R.; Goormaghtigh, E.; Greathouse, D. V.; Koeppe, R. E.; Kruijtzter, J. A. W.; Liskamp, R. M. J.; de Kruijff, B.; Killian, J. A. *Biochemistry* **2001**, *40*, 5000–5010.
- (14) Harzer, U.; Bechinger, B. *Biochemistry* **2000**, *39*, 13106–13114.
- (15) Kandasamy, S.; Larson, R. *Biophys. J.* **2006**, *90*, 2326–2343.
- (16) Petrache, H. I.; Zuckerman, D. M.; Sachs, J. N.; Killian, J. A.; Koeppe, R. E.; Woolf, T. B. *Langmuir* **2002**, *18*, 1340–1351.
- (17) Ren, J. H.; Lew, S.; Wang, J. Y.; London, E. *Biochemistry* **1999**, *38*, 5905–5912.
- (18) Ren, J. H.; Lew, S.; Wang, Z. W.; London, E. *Biochemistry* **1997**, *36*, 10213–10220.
- (19) Webb, R. J.; East, J. M.; Sharma, R. P.; Lee, A. G. *Biochemistry* **1998**, *37*, 673–679.
- (20) Esteban-Martin, S.; Salgado, J. *Biophys. J.* **2007**, *93*, 4278–4288.
- (21) Ozdirekcan, S.; Etchebest, C.; Killian, J. A.; Fuchs, P. F. *J. Am. Chem. Soc.* **2007**, *129*, 15174–15181.
- (22) Ozdirekcan, S.; Rijkers, D. T. S.; Liskamp, R. M. J.; Killian, J. A. *Biochemistry* **2005**, *44*, 1004–1012.
- (23) Strandberg, E.; Esteban-Martin, S.; Salgado, J.; Ulrich, A. S. *Biophys. J.* **2009**, *96*, 3223–3232.
- (24) Strandberg, E.; Killian, J. A. *FEBS Lett.* **2003**, *544*, 69–73.
- (25) Taulier, N.; Nicot, C.; Waks, M.; Hodges, R. S.; Ober, R.; Urbach, W. *Biophys. J.* **2000**, *78*, 857–865.
- (26) Taulier, N.; Waks, M.; Gulik-Krzywicki, T.; Urbach, W. *Europhys. Lett.* **2002**, *59*, 142–148.
- (27) Saffman, P. G.; Delbruck, M. *Proc. Natl. Acad. Sci. U.S.A.* **1975**, *72*, 3111–3113.
- (28) Frey, S.; Tamm, L. K. *Biochem. J.* **1990**, *272*, 713–719.
- (29) Kenworthy, A. K.; Nichols, B. J.; Rimmert, C. L.; Hendrix, G. M.; Kumar, M.; Zimmerberg, J.; Lippincott-Schwartz, J. *J. Cell Biol.* **2004**, *165*, 735–746.
- (30) Kucik, D. F.; Elson, E. L.; Sheetz, M. P. *Biophys. J.* **1999**, *76*, 314–322.
- (31) Suzuki, K.; Ritchie, K.; Kajikawa, E.; Fujiwara, T.; Kusumi, A. *Biophys. J.* **2005**, *88*, 3659–3680.
- (32) Lee, C. C.; Petersen, N. O. *Biophys. J.* **2003**, *84*, 1756–1764.
- (33) Gambin, Y.; Lopez-Esparza, R.; Reffay, M.; Sierrecki, E.; Gov, N. S.; Genest, M.; Hodges, R. S.; Urbach, W. *Proc. Natl. Acad. Sci. U.S.A.* **2006**, *103*, 2098–2102.
- (34) Naji, A.; Levine, A. J.; Pincus, P. A. *Biophys. J.* **2007**, *93*, L49–L51.
- (35) Kriegsmann, J.; Gregor, I.; von der Hocht, I.; Klare, J. P.; Engelhard, M.; Enderlein, J.; Fitter, J. *Chembiochem* **2009**, *10*, 1823–1829.
- (36) Ramadurai, S.; Holt, A.; Krasnikov, V.; van den Bogaart, G.; Killian, J. A.; Poolman, B. *J. Am. Chem. Soc.* **2009**, *131*, 12650–12656.
- (37) Liu, F.; Lewis, R.; Hodges, R. S.; McElhaney, R. N. *Biochemistry* **2002**, *41*, 9197–9207.
- (38) Liu, F.; Lewis, R.; Hodges, R. S.; McElhaney, R. N. *Biophys. J.* **2004**, *87*, 2470–2482.
- (39) Sereida T. J.; Mant C. T.; Quinn A. M.; Hodges R. S. *J. Chromatogr.* **1993**, *646*, 17–30.
- (40) Roux, D.; Coulon, C.; Cates, M. E. *J. Phys. Chem.* **1992**, *96*, 4174–4187.
- (41) Davoust, J.; Devaux, P. F. *J. Cell Biol.* **1982**, *95*, A459–A459.
- (42) Davoust, J.; Devaux, P. F.; Leger, L. *EMBO J.* **1982**, *1*, 1233–1238.
- (43) Gambin, Y.; Massiera, G.; Ramos, L.; Ligoure, C.; Urbach, W. *Phys. Rev. Lett.* **2005**, *94*, 110602–110607.
- (44) Killian, J. A.; von Heijne, G. *Trends Biochem. Sci.* **2000**, *25*, 429–434.
- (45) Doeven, M. K.; Folgering, J. H. A.; Krasnikov, V.; Geertsma, E. R.; van den Bogaart, G.; Poolman, B. *Biophys. J.* **2005**, *88*, 1134–1142.
- (46) Girard, P.; Pecreaux, J.; Lenoir, G.; Falson, P.; Rigaud, J. L.; Bassereau, P. *Biophys. J.* **2004**, *87*, 419–429.
- (47) Kahya, N.; Pecheur, E. I.; de Boeij, W. P.; Wiersma, D. A.; Hoekstra, D. *Biophys. J.* **2001**, *81*, 1464–1474.
- (48) Park, S. H.; Opella, S. J. *J. Mol. Biol.* **2005**, *350*, 310–318.
- (49) Koehorst, R. B.; Spruijt, R. B.; Vergeldt, F. J.; Hemminga, M. A. *Biophys. J.* **2004**, *87*, 1445–1455.
- (50) Venturoli, M.; Smit, B.; Sperotto, M. M. *Biophys. J.* **2005**, *88*, 1778–1798.
- (51) Abrecht, H.; Goormaghtigh, E.; Ruysschaert, J. M.; Homble, F. *J. Biol. Chem.* **2000**, *275*, 40992–40999.
- (52) Bechinger, B.; Ruysschaert, J. M.; Goormaghtigh, E. *Biophys. J.* **1999**, *76*, 552–563.